

MOX-Report No. 12/2007

An Accurate and Efficient Semi-Implicit Method for Section Averaged Free Surface Flow Modelling

ALBERTO DEPONTI, LUCA BONAVENTURA,
GIORGIO ROSATTI, GIULIA GAREGNANI

MOX, Dipartimento di Matematica "F. Brioschi"
Politecnico di Milano, Via Bonardi 29 - 20133 Milano (Italy)

mox@mate.polimi.it

<http://mox.polimi.it>

An Accurate and Efficient Semi-Implicit Method for Section Averaged Free Surface Flow Modelling*

Alberto Deponti^(#), Luca Bonaventura^(b),
Giorgio Rosatti^(#), Giulia Garegnani^(b)

10th July 2007

^(b) MOX – Modelling and Scientific Computing,
Dipartimento di Matematica “F. Brioschi”, Politecnico di Milano
Via Bonardi 9, 20133 Milano, Italy
`luca.bonaventura@polimi.it`

^(#) CUDAM – Centro Universitario per la Difesa Idrologica dell’Ambiente Montano,
Dipartimento di Ingegneria Civile e Ambientale, Università degli Studi di Trento
Mesiano di Povo, 38050 (TN), Italy
`deponi@ing.unitn.it`, `rosatti@ing.unitn.it`

Keywords: Semi-implicit discretizations, semi-Lagrangian discretizations, computational hydraulics, shallow water equations, Saint Venant equations.

AMS Subject Classification: 35L60, 35Q35, 76D99, 65M06, 65Z05

*This work is dedicated to the memory of Fausto Saleri, who warmly encouraged it and strongly supported us throughout its development.

Abstract

An accurate, efficient and robust numerical method for the solution of the section averaged equations of open channel flow is presented and discussed. The method allows for river sections of arbitrary shape and for arbitrary bottom topography. The continuity equation is formulated in a conservative fashion, while a non conservative form is chosen for the momentum equation, thus avoiding the need for well balanced schemes to handle rapidly varying bathymetry. In order to achieve unconditional stability with respect to flow celerity, a semi-implicit time discretization is introduced, which requires the solution of a weakly nonlinear system for the free surface at each time step by a fixed point iteration technique. A semi-Lagrangian discretization is introduced, to achieve full unconditional stability and increase efficiency at no accuracy loss in subcritical flow regimes. An appropriate upwind discretization is also introduced for the momentum equation, which allows to recover correct solutions also in presence of discontinuities and strong gradients. Numerical experiments show that the semi-Lagrangian method yields indeed accurate results also in the case of stationary hydraulic jumps. The model is validated in a wide range of idealised test cases, highlighting its accuracy and efficiency characteristics, especially for long time range simulations of subcritical river flow. Finally, a first model validation on realistic data is presented, concerning simulations of flooding events of the Adda river.

1 Introduction

Mathematical modelling of river flow is usually based on the vertically averaged Saint-Venant equations, which can be written in one or two dimensions to express the conservation laws of mass and momentum for water flow. The numerical solution of these equations has attracted great attention in the last couple of decades. A review of numerical schemes for these equations can be found for example in [23]. Since the Saint-Venant equations are equivalent to the Euler equations of gas dynamics in the inviscid case, many numerical methods rely on the huge body of results on nonlinear conservation laws for applications in high Mach/Froude number regimes. The use of the fully conservative formulation is indeed necessary for accurate simulations of hydraulic jumps and discontinuous solutions, such as those that arise in dam break simulations. However, in presence of strongly varying bathymetry, fully conservative formulations of the momentum equation need to be supplemented with special treatment of the bathymetric source terms, which in some situations (e.g. still water) may balance almost exactly the momentum flux. A number of results are now available on well balanced schemes for the shallow water equations (see e.g. [11], [19], [20], [21], [24], [26]), but application of these results to section averaged models with arbitrarily shaped sections is not straightforward.

Furthermore, the numerical methods based on explicit, flux-form time discretizations, must usually comply with CFL-type stability restrictions, which require the use of relatively small time steps and increase substantially the computational cost. This is especially true whenever long time range river flow simulations have to be performed, which is often the case in many important applications, such as those to the computation of river flow scenarios including sediment transport models or based on long term precipitation patterns.

For these reasons, in this paper we describe a semi-implicit method that is unconditionally stable with respect to the flow celerity. Full unconditional stability is achieved by coupling to a semi-Lagrangian method for the advective terms. Alternatively, since the semi-Lagrangian discretization can produce inaccurate results in presence of unsteady shocks, an upwind based scheme for momentum advection is also proposed, which is stable under a generally milder CFL condition based on the flow velocity. The semi-implicit, semi-Lagrangian method is based on the approaches proposed in [6], [7], [18] for the two dimensional shallow water equations. In these formulations, the momentum equation is not in full flux-form, but expresses rather the hydrostatic pressure gradient as a function of the free surface, thus avoiding the presence of bathymetric source terms and the need for well balanced discretizations. Furthermore, these time discretization approaches yield unconditionally stable numerical methods, whose time step can be chosen based on accuracy considerations, rather than stability restrictions related to the flow celerity. Similar applications of the semi-implicit technique to one dimensional river flow had already been proposed in [3], [8], but in those papers no extensive validation of the method was presented and the numerical results only concerned rather low Courant number cases.

In previous implementations, this method has been used successfully by some of the authors over the last ten years to carry out a wide range of river hydraulics simulations. In particular, the method was used for sediment transport simulations and river morphology studies, in which very long time integrations had to be performed. The stable and accurate time discretization technique allowed to reduce substantially the computational costs, by employing time steps several times larger than those that would have been feasible for standard explicit discretizations.

Another peculiarity of the method is that of being based on the section averaged equations of river flow, thus allowing to handle arbitrarily shaped sections and to recover some two dimensional information across each river section at reduced computational cost. The use of arbitrarily shaped sections is also expected to allow for easier derivation of hybrid 1D-2D models along the lines of [16], [17], which is one of the planned extensions of the model presented here.

In this paper, the method is presented and validated for the case of fixed bed flow, while the mobile bed case and the coupling to sediment transport models will be considered in forthcoming works. In particular, our aim is to emphasise the superior efficiency and robustness of the present approach, which does not entail any essential loss in accuracy for the simulation of subcritical and supercritical river flow regimes. For this purpose, the results obtained with the proposed methods have been compared to those of more standard techniques, including explicit time discretization of the same equations in fully conservative form.

In section 2, the model equations are introduced and discussed. In section 3, two different methods for computing friction and Coriolis coefficients are presented. In section 4, the numerical method is presented. In section 5, the solution of the nonlinear system is described. In section 6, the model results on a number of idealised test cases are presented, along with the results obtained by different numerical methods on the same tests. In section 7, we present the results of a first attempt at model validation based on real data, in which flooding scenarios for the Adda river have been simulated.

2 The section averaged model equations for open channel flow

The section averaged equations for fixed bed, free surface channel flow can be written in conservative form (see e.g. [5])

$$\frac{\partial A_l}{\partial t} + \frac{\partial Q_l}{\partial x} = 0, \quad (1)$$

$$\frac{\partial Q_l}{\partial t} + \frac{\partial}{\partial x} \left(\beta \frac{Q_l^2}{A_l} + gI_1 \right) = gA_l(S_0 - S_f) + gI_2. \quad (2)$$

Equations (1)–(2) express the conservation of liquid mass and momentum. Here, A_l denotes the area of the wet cross section, Q_l the liquid discharge, β the Coriolis averaging coefficient, I_1 the first moment of the wet cross section with respect to the free surface, I_2 the spatial variation of the first moment, S_0 the bottom slope, S_f the friction slope (see figure 1 for a sketch

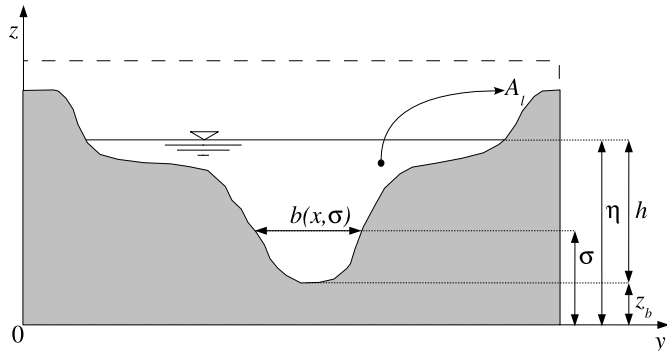


Figure 1: Sketch of the generic river cross section and of the main model variables.

of the generic cross section). Terms S_0 , I_1 and I_2 depend on the channel geometry and are defined by:

$$S_0 = -\frac{\partial z_b}{\partial x}, \quad (3)$$

$$I_1 = \int_0^h (h - \sigma) b(x, \sigma) d\sigma, \quad (4)$$

$$I_2 = \int_0^h (h - \sigma) \frac{\partial b(x, \sigma)}{\partial x} d\sigma, \quad (5)$$

where $h = \eta - z_b$ is the water depth, η and z_b are the elevations of the free surface and of the cross section lowest point above a fixed reference level, respectively, $b(x, \sigma)$ is the width-depth relationship. With simple calculations it is possible to prove that

$$\frac{\partial}{\partial x} (gI_1) - gI_2 + gA_l S_0 = gA_l \frac{\partial \eta}{\partial x}. \quad (6)$$

The Coriolis averaging coefficient β in the momentum conservation equation (2) takes into account the effects due to the two dimensional variability of the local velocity u across the section and is defined by

$$\beta = \frac{1}{A_l} \int_{A_l} \frac{u^2}{U^2} da, \quad (7)$$

where $U = Q_l/A_l$ is the section averaged velocity. Assuming that the average bottom friction $\bar{\tau}_0$ is balanced locally by the gravity force $\rho g R_h S_f$ (where $R_h = A_l/C_w$ is the hydraulic radius and C_w the length of the wet

contour), the term $-gA_l S_f$ can be rewritten as:

$$-gA_l S_f = -\frac{\bar{\tau}_0}{\rho} C_w. \quad (8)$$

Furthermore, the bottom stress can be expressed as a function of liquid discharge Q_l using the Chézy–Tadini formula

$$\frac{\bar{\tau}_0}{\rho} = U |U| \frac{g}{\chi^2} \quad (9)$$

where χ is the Chézy roughness parameter; this yields

$$-\frac{\bar{\tau}_0}{\rho} C_w = -U |U| \frac{g}{\chi^2} C_w = -g |U| \frac{Q_l C_w}{\chi^2 A_l} = -g |U| \frac{Q_l}{\chi^2} R_h = \alpha_1 Q_l \quad (10)$$

where $\alpha_1 = -(g|U|)/(\chi^2 R_h)$. Substituting (6) and (10) into (2) it is possible to write the quasi-conservative form of the momentum equation:

$$\frac{\partial Q_l}{\partial t} + \frac{\partial}{\partial x} \left(\beta \frac{Q_l^2}{A_l} \right) + g A_l \frac{\partial \eta}{\partial x} = -\alpha_1 Q_l. \quad (11)$$

When an Eulerian discretization method is employed for momentum advection, equations (1) and (11) are discretized and solved.

For the purpose of the formulation of the semi-Lagrangian numerical method, the momentum equation (11) is rewritten in advective form as

$$\frac{\partial Q_l}{\partial t} + \beta U \frac{\partial Q_l}{\partial x} + g A_l \frac{\partial \eta}{\partial x} = -(\alpha_1 + \alpha_2) Q_l \quad (12)$$

where $\alpha_2 = \partial(\beta U)/\partial x$; for application of this numerical technique, equations (1) and (12) are discretized and solved. Both formulations can be easily combined in a single numerical model, in which either option can be chosen for the advective and frictional terms.

3 Computation of friction and Coriolis coefficients

In general cases, bottom friction varies along the cross section due to different sediment characteristics and due to the presence of vegetation. This can be represented by dividing each cross section into N subareas having different local values of Chézy coefficient χ_j or of the Strickler coefficient K_j (the label j refers to local values). A bulk friction coefficient is computed for each cross section, accounting for variable roughness along the cross section. Two different methods for computing such bulk roughness coefficient are implemented: the Einstein–Horton method and the Lotter method. A complete description of the two methods can be found in [9]. The former performs better on compact cross sections, while the latter performs better on non-compact cross sections. If the roughness is described by means of local Strickler coefficient, the bulk coefficient K is computed first and then the bulk Chézy coefficient is computed using the relation

$$\chi = K R_h^{1/6}. \quad (13)$$

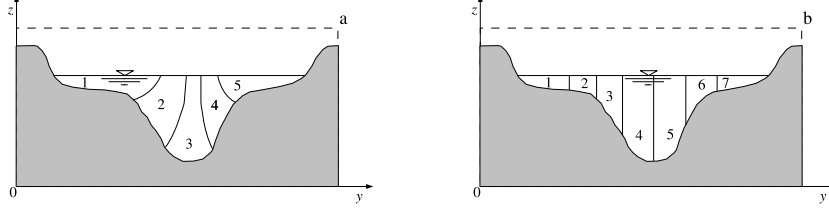


Figure 2: Division of the cross section into subareas using the Einstein-Horton method (a) and the Lotter method (b).

In the Einstein–Horton method the cross section is divided into different subareas having the same velocity U (see figure 2.a). By applying the Chézy–Tadini formula (9) both locally on each subareas and globally on the whole cross section, it is possible to formulate the following expression for the bulk Chézy coefficient:

$$\chi = \sqrt{\frac{C_w}{\sum_{j=1}^N (C_w)_j / \chi_j^2}}. \quad (14)$$

In a similar manner, by applying both locally and globally the Strickler formula

$$u = KR_h^{2/3} \sqrt{S_f}, \quad (15)$$

it is possible to formulate the following expression for the bulk Strickler coefficient

$$K = \left[\frac{C_w}{\sum_{j=1}^N (C_w)_j / K_j^{-3/2}} \right]^{2/3}. \quad (16)$$

In the Lotter method, the cross section is divided into subareas separated by vertical lines and the hypothesis of having the same velocity in each subarea is dropped. In this way the local and global application of the Chézy–Tadini formula (9) leads to the following expression for the bulk Chézy coefficient:

$$\chi = \frac{\sum_{j=1}^N \chi_j (A_l)_j^{3/2} (C_w)_j^{-1/2}}{A_l^{3/2} C_w^{-1/2}}. \quad (17)$$

The local and global application of the Strickler formula (15) leads to the following expression for the bulk Strickler coefficient:

$$K = \frac{\sum_{j=1}^N K_j (A_l)_j^{5/3} (C_w)_j^{-2/3}}{A_l^{5/3} C_w^{-2/3}}. \quad (18)$$

In both cases, the hydraulic radius is defined by $R_h = A_l/C_w$. The Coriolis averaging coefficient β is computed by the following discretization of (7):

$$\beta = \frac{1}{A_l} \sum_{j=1}^N \frac{u_j^2 (A_l)_j}{U^2}. \quad (19)$$

In the Einstein–Horton method $u_j = U$, hence $\beta = 1$. In the Lotter method $u_j \neq U$, hence it is possible to compute β by substituting (9) and (15) into (19) obtaining

$$\beta = \frac{\sum_{j=1}^N \chi_j^2 (A_l)_j^2 (C_w)_j^{-1}}{\chi^2 A_l^2 C_w^{-1}} \quad (20)$$

and

$$\beta = \frac{\sum_{j=1}^N K_j^2 (A_l)_j^{7/3} (C_w)_j^{-4/3}}{K^2 A_l^{7/3} C_w^{-4/3}}, \quad (21)$$

respectively.

4 The numerical method

Equations (1)–(12), or, alternatively, equations (1)–(11), are discretized on a staggered computational grid, such that the liquid area and free surface height are defined at the integer nodes x_i , while the liquid discharge is defined at the half integer nodes $x_{i+1/2} = (x_i + x_{i+1})/2$. The node distribution is arbitrary and the node spacings are defined as $\Delta x_i = x_{i+1/2} - x_{i-1/2}$ and $\Delta x_{i+1/2} = x_{i+1} - x_i$, respectively.

The free surface gradients and the frictional terms in the momentum equation are discretized in time by the ϑ -method. The nonlinear dependence of these terms on η (through A_l) and Q_l , respectively, is linearised in time by considering these quantities computed at time level n . As a result, one obtains the discrete momentum equation

$$\begin{aligned} (Q_l)_{i+1/2}^{n+1} &- \mathcal{F}_{i+1/2} [(Q_l)^n] \\ &+ \vartheta \Delta t g (A_l)_{i+1/2}^n \frac{\eta_{i+1}^{n+1} - \eta_i^{n+1}}{\Delta x_{i+1/2}} \\ &+ \vartheta \Delta t \alpha_{i+1/2}^n (Q_l)_{i+1/2}^{n+1} = 0. \end{aligned} \quad (22)$$

Here, $\mathcal{F}_{i+1/2} [(Q_l)^n]$ denotes the sum of all terms discretized explicitly in time. Furthermore, two different techniques are implemented for the interpolation of the liquid area A_l values at nodes $i + 1/2$: a quadratic interpolation on an upwind biased stencil and an upwind weighted linear interpolation of the form $(A_l)_{i+1/2} = p(A_l)_u + (1-p)(A_l)_d$, where indexes u and d refer to upwind and downwind points respectively. p is the upwind weight that can be chosen depending on the typical Froude number. If the semi-Lagrangian discretization is employed, this term is given by

$$\begin{aligned} \mathcal{F}_{i+1/2} [(Q_l)^n] &= \left[(Q_l)_{i+1/2}^n - (1-\vartheta) \Delta t g (A_l)_{i+1/2}^n \frac{\eta_{i+1}^n - \eta_i^n}{\Delta x_{i+1/2}} \right. \\ &\left. - (1-\vartheta) \Delta t \alpha_{i+1/2}^n (Q_l)_{i+1/2}^n \right]_* \end{aligned} \quad (23)$$

where $[\cdot]_*$ denotes a quantity interpolated at the foot of the streamline computed based on the velocity field βU . In the present work, a cubic interpolation is used for the reconstruction of the momentum values at the foot of the streamline. In case of the upwind discretization,

$$\begin{aligned}\mathcal{F}_{i+1/2} [(Q_l)^n] &= (Q_l)_{i+1/2}^n - \Delta t \frac{F_{i+1}^n - F_i^n}{\Delta x_{i+1/2}} \\ &- (1 - \vartheta) \Delta t g(A_l)_{i+1/2}^n \frac{\eta_{i+1}^n - \eta_i^n}{\Delta x_{i+1/2}} \\ &- (1 - \vartheta) \Delta t \alpha_{i+1/2}^n (Q_l)_{i+1/2}^n,\end{aligned}\quad (24)$$

where F_i denotes the upwind based discretization of the momentum flux in equation (11). Note that the definition of the effective friction coefficient $\alpha_{i+1/2}$ changes according to the discretization method employed for the momentum advection term (see remark at the end of the previous section). Rearranging so as to solve for $(Q_l)_{i+1/2}^{n+1}$ one obtains

$$\begin{aligned}(Q_l)_{i+1/2}^{n+1} &= \frac{\mathcal{F}_{i+1/2} [(Q_l)^n]}{(1 + \alpha_{i+1/2}^n \vartheta \Delta t)} \\ &- \frac{\vartheta \Delta t}{\Delta x_{i+1/2}} \frac{g(A_l)_{i+1/2}^n}{(1 + \alpha_{i+1/2}^n \vartheta \Delta t)} (\eta_{i+1}^{n+1} - \eta_i^{n+1}).\end{aligned}\quad (25)$$

Concerning the continuity equation, we consider the control volume i comprised between the staggered momentum nodes $i - 1/2$ and $i + 1/2$; integrating the continuity equation (1) over this control volume one obtains

$$\begin{aligned}(V_l)_i^{n+1} &- (V_l)_i^n + \vartheta \Delta t [(Q_l)_{i+1/2}^{n+1} - (Q_l)_{i-1/2}^{n+1}] \\ &+ (1 - \vartheta) \Delta t [(Q_l)_{i+1/2}^n - (Q_l)_{i-1/2}^n] = 0\end{aligned}\quad (26)$$

where $(V_l)_i$ denotes the liquid volume between nodes $i - 1/2$ and $i + 1/2$. It should be remarked that, if an arbitrary section shape is considered, this quantity depends in a nonlinear fashion on the free surface value η_i^{n+1} . Substituting now equation (25) in (26) one obtains

$$\begin{aligned}(V_l)_i^{n+1} &- \frac{\vartheta^2 \Delta t^2}{\Delta x_{i+1/2}} \frac{g(A_l)_{i+1/2}^n}{(1 + \alpha_{i+1/2}^n \vartheta \Delta t)} (\eta_{i+1}^{n+1} - \eta_i^{n+1}) \\ &+ \frac{\vartheta^2 \Delta t^2}{\Delta x_{i-1/2}} \frac{g(A_l)_{i-1/2}^n}{(1 + \alpha_{i-1/2}^n \vartheta \Delta t)} (\eta_i^{n+1} - \eta_{i-1}^{n+1}) = \mathcal{B}_i^n\end{aligned}\quad (27)$$

where

$$\begin{aligned}\mathcal{B}_i^n &= (V_l)_i^n - (1 - \vartheta) \Delta t [(Q_l)_{i+1/2}^n - (Q_l)_{i-1/2}^n] \\ &- \vartheta \Delta t \left[\frac{\mathcal{F}_{i+1/2} [(Q_l)^n]}{(1 + \alpha_{i+1/2}^n \vartheta \Delta t)} - \frac{\mathcal{F}_{i-1/2} [(Q_l)^n]}{(1 + \alpha_{i-1/2}^n \vartheta \Delta t)} \right].\end{aligned}\quad (28)$$

Equations (27) constitute a weakly nonlinear system that can be solved after prescribing appropriate boundary conditions. In the subcritical regime,

the characteristics of the hyperbolic system have opposite signs, so that a condition on the discharge has to be specified at one boundary (usually the inflow one) and a condition on the elevation or on the water depth has to be specified at the other boundary (usually the outflow one). In the supercritical regime, both the characteristics of the hyperbolic system are positive, so that a condition on the discharge and a condition on the surface elevation or on the water depth have to be imposed at the upstream inflow boundary. This is consistent with the analysis carried out in [10] for the mobile bed case. Once boundary conditions have been assigned, this nonlinear system can be rewritten in vector notation as

$$\mathbf{V}_l(\boldsymbol{\eta}) + \mathbf{M}\boldsymbol{\eta} = \mathbf{b}. \quad (29)$$

Here, $\boldsymbol{\eta}$ denotes a vector unknown whose components are the values η_i^{n+1} , $\mathbf{V}_l(\boldsymbol{\eta})$ denotes a vector valued function whose components are the liquid volumes $(V_l)_i^{n+1}$, \mathbf{M} is a symmetric tridiagonal matrix and the components of the right hand side \mathbf{b} are given by the terms \mathcal{B}_i^n .

5 Solution of the nonlinear system

The numerical method described in the previous sections requires, at each time step, the solution of the weakly nonlinear system (29). Along the lines of [4], [13], it can be shown that, under mild regularity assumption on the functions $V_l(\eta)_i$, this system admits a unique solution that can be computed by a fixed point method. More specifically, we will require that $V_l(\eta)_i$, is given for each i by a Lipschitz continuous function of η . This is a reasonable assumption, since it amounts to require that the liquid area $A_l = \partial(V_l)_i/\partial\eta$ is bounded, i.e. the flow is always contained in the river bed and no flooding of an infinitely large river bank is taking place. Under this hypothesis, it is easy to verify that the fixed point iterations

$$\begin{aligned} \mathbf{M}\boldsymbol{\eta}^{(k+1)} &= \mathbf{b} - \mathbf{V}_l(\boldsymbol{\eta}^{(k)}) \\ \boldsymbol{\eta}^{(0)} &= \boldsymbol{\eta}^n \end{aligned} \quad (30)$$

converge to the solution of (29) provided that

$$\|\mathbf{M}^{-1}\| \left\| \frac{\partial \mathbf{V}_l}{\partial \boldsymbol{\eta}} \right\| < 1$$

is satisfied, where $\|\cdot\|$ denotes the discrete ℓ^2 norm and the index k denotes the generic iteration step. Since \mathbf{M} depends on the time step, this condition is always satisfied for sufficiently small Δt . Furthermore, in order to speed up convergence of the fixed point iterations, we introduce a slightly modified fixed point problem. We define $\mathbf{V}'_l(\boldsymbol{\eta}) = \text{diag}(\partial(V_l)_1/\partial\eta, \dots, \partial(V_l)_N/\partial\eta)$ and reformulate (30) as

$$\begin{aligned} [\mathbf{M} + \mathbf{V}'_l(\boldsymbol{\eta}^{(0)})] \boldsymbol{\eta}^{(k+1)} &= \mathbf{b} - \mathbf{V}_l(\boldsymbol{\eta}^{(k)}) + \mathbf{V}'_l(\boldsymbol{\eta}^{(0)})\boldsymbol{\eta}^{(k)} \\ \boldsymbol{\eta}^{(0)} &= \boldsymbol{\eta}^n. \end{aligned} \quad (31)$$

It is immediate that also the limit of (31) is a solution of (29), while the sufficient condition for its convergence is now relaxed to

$$\left\| \left[\mathbf{M} + \mathbf{V}'_l(\boldsymbol{\eta}^{(0)}) \right]^{-1} \right\| \left\| \mathbf{V}'_l(\boldsymbol{\eta}^{(0)}) - \frac{\partial \mathbf{V}_l}{\partial \boldsymbol{\eta}} \right\| < 1.$$

6 Model validation: idealised tests

In order to validate the numerical model described in the previous sections, a number of numerical tests have been carried out, concerning either benchmark cases with analytic solutions or idealised versions of problem often encountered in practice. In general, the ϑ parameter of the semi-implicit time discretization was taken equal to 0.6. All the tests were performed using both the semi-Lagrangian method and the Eulerian method using the upwind scheme for the discretization of the momentum advection. Courant numbers based on velocity and celerity are defined as

$$C_{vel} = \frac{|\beta U| \Delta t}{\Delta x}, \quad C_{cel} = \frac{(|\beta U| + \sqrt{gh}) \Delta t}{\Delta x}.$$

The time discretization step Δt is chosen for each time level so as to yield an assigned maximum value of C_{vel} ; for the semi-Lagrangian method, values larger than one were generally chosen.

In those simulations aimed at reproducing a steady state solution, convergence to steady state was considered to be achieved based on the criterion

$$\frac{\|\eta^{n+1} - \eta^n\|}{\|\eta^{n+1}\|} < \varepsilon,$$

where $\|\cdot\|$ denotes the discrete ℓ^2 norm and ε is a tolerance parameter. Friction and Coriolis coefficients were computed using the Einstein–Horton method in all the tests where a rectangular cross section was considered and using the Lotter method in the test where an arbitrary non-compact cross section was considered.

In the first test, a dam break problem was considered in order to highlight the limitations of the semi-Lagrangian method for shock wave propagation. As expected from the theory (see e.g. [14] and the references therein), the position of the shock is not correctly captured by the non-conservative semi-Lagrangian scheme. On the other hand, when using the upwind scheme for the momentum advection terms and the quasi-conservative formulation given by equations (1) and (11), the correct propagation speed was obtained. Furthermore, in all the other tests performed, even in presence of strong hydraulic jumps, the semi-Lagrangian scheme yields results that are very close, both qualitatively and quantitatively, to those of the upwind method, while reducing substantially the computational cost; for this reason, for these tests only the results of the semi-Lagrangian method are presented. Moreover, in all the tests, apart from the dam break and the tidal wave test, the liquid area is interpolated in points $i + 1/2$ by means of an upwind biased quadratic interpolation.

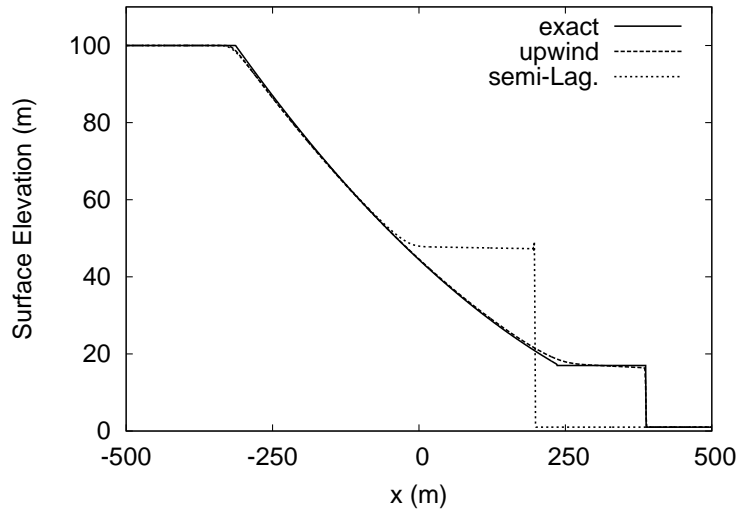


Figure 3: Dam break test: Free surface elevation 10 s after the dam break event.

6.1 Dam break in a channel with rectangular cross section

A dam break event in a rectangular section channel with frictionless bed is considered in this test. The domain is discretized into 1 001 uniformly spaced sections with $\Delta x = 1$ m. The initial conditions prescribe null discharge and a water depth equal to 100 m behind the dam and equal to 1 m past the dam. The boundary conditions prescribe a null discharge at the inflow boundary and a constant water depth of 1 m at the outflow boundary. A 10 s simulation is performed. As the dam breaks down, a shock wave and a rarefaction wave start to travel in opposite directions with celerity $u \pm \sqrt{gh}$ (see e.g. [22]). This is a challenging test for the model, since neither the equation formulation nor its numerical approximation are in fully conservative form.

Both the upwind and the semi-Lagrangian method are used in this test. For this test the liquid area is interpolated in points $i + 1/2$ by means of an upwind weighted interpolation with weight $p = 0.9$. The upwind scheme is used with $C_{vel} = 0.5$ and $C_{cel} = 0.8$ in order to achieve a stable and correct numerical solution. The semi-Lagrangian method is used with values of C_{vel} up to 0.8 and C_{cel} up to 1.6. The free surface elevations computed by the two different discretizations are presented in figure 3 and compared to the analytical solution. As expected, the semi-Lagrangian method fails in predicting the correct amplitude and speed of the shock wave, while for the upwind scheme both wave speed and amplitude are in good agreement with the analytical solution.

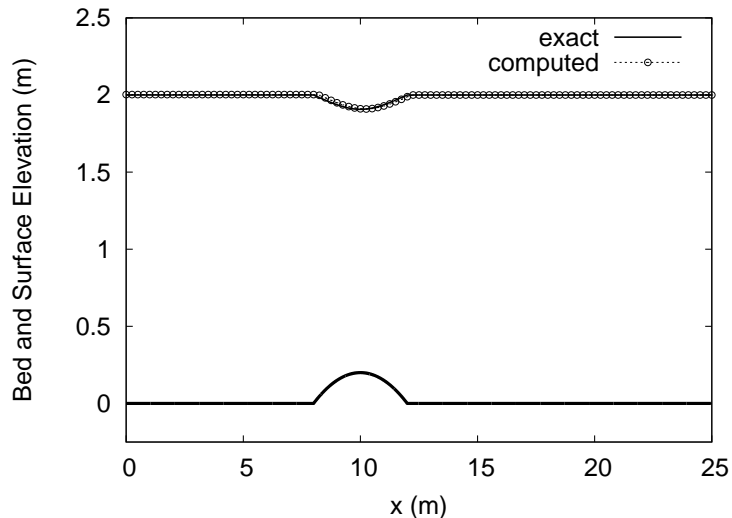


Figure 4: Subcritical flow over a bump: free surface elevation.

6.2 Steady flow over a bump in a rectangular section channel: inviscid case

The steady flow over a parabolic bump has also been considered. This is a classical test problem considered by various authors ([11], [12], [24], [26]); moreover, exact solutions can be computed using the Bernoulli theorem and the principle of momentum conservation. A 25 m long and 1 m wide channel with rectangular section is considered; the bottom topography is given by:

$$z_b(x) = \begin{cases} 0.2 - 0.05(x - 10)^2 & 8 < x < 12 \\ 0 & \text{otherwise} \end{cases} \quad (32)$$

In these tests, no frictional effect is considered. The flow is considered in either subcritical regime or in transcritical regime, with or without a steady shock. The boundary conditions for the three regimes are:

- subcritical flow
inflow: $Q_l = 4.42 \text{ m}^3/\text{s}$, outflow: $h = 2 \text{ m}$
- transcritical flow with a steady shock
inflow: $Q_l = 0.18 \text{ m}^3/\text{s}$, outflow: $h = 0.33 \text{ m}$
- transcritical flow without shock
inflow: $Q_l = 1.53 \text{ m}^3/\text{s}$, outflow: $h = 0.66 \text{ m}$ (only when the flow is subcritical)

In figures 4–6, the computed free surface elevations are compared to the exact solutions. The tolerance for the steady state is $\varepsilon = 10^{-5}$ and the space discretization is $\Delta x = 0.25 \text{ m}$. In the case of subcritical flow $C_{vel} = 1.5$ is used, corresponding to a maximum celerity Courant number $C_{cel} = 4.1$; in the case of transcritical flow with a steady shock $C_{vel} = 2.0$ is used, corresponding to a maximum celerity Courant number $C_{cel} = 3.6$; in the case of transcritical flow without a shock $C_{vel} = 0.6$ is used, corresponding to

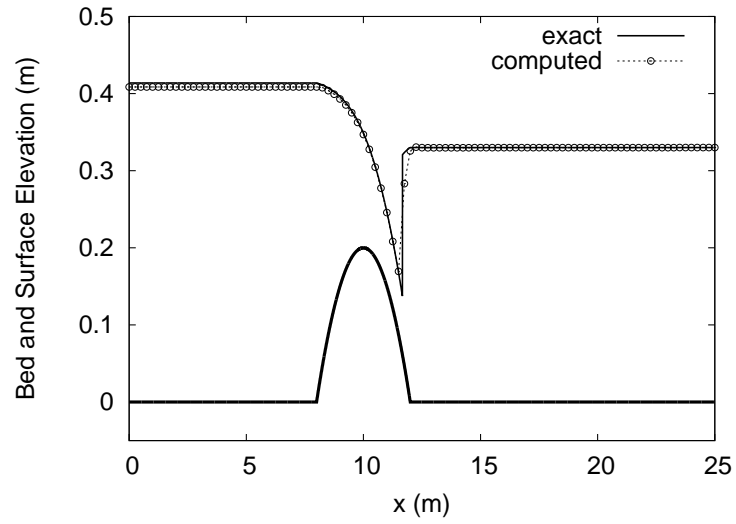


Figure 5: Transcritical flow over a bump in presence of a shock: free surface elevation.

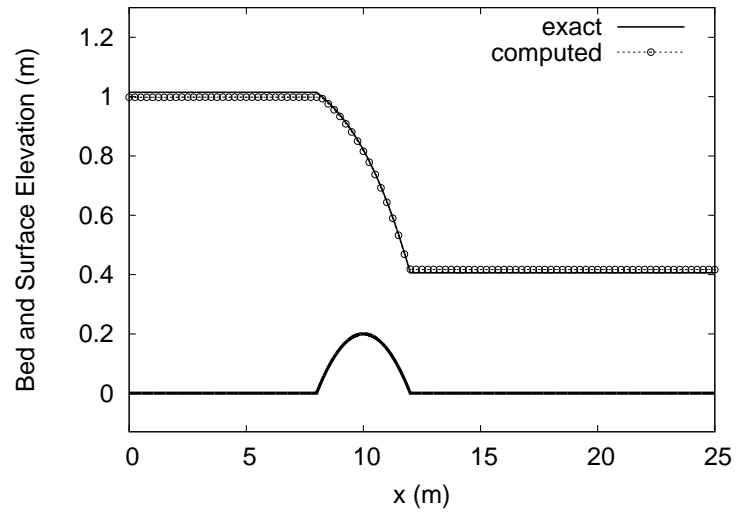


Figure 6: Transcritical flow over a bump in absence of a shock: free surface elevation.

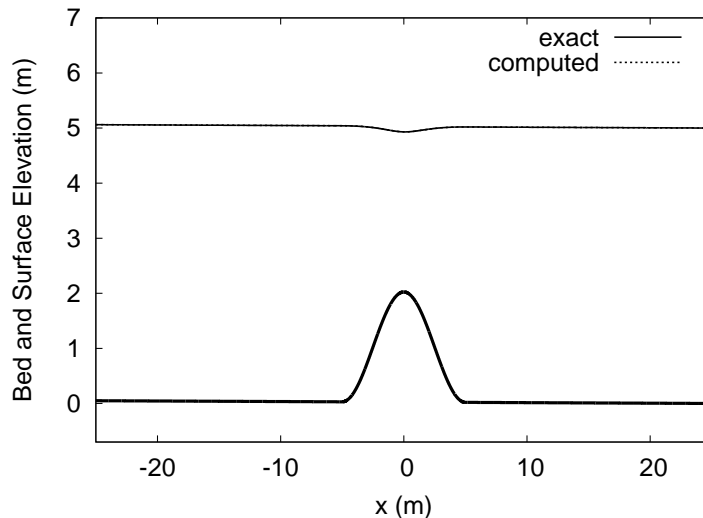


Figure 7: Subcritical flow over a bump with friction: free surface elevation.

a maximum celerity Courant number $C_{cel} = 1.0$. These tests demonstrate the capability of the method to capture the exact solution even in the cases of transcritical regimes with or without a steady shock, in spite of being based on the non-conservative form of the Saint-Venant equations.

6.3 Steady flow over a bump: frictional effects

In these tests the steady flow over a sinusoidal bump with friction is considered. The inclusion of bottom inclination and friction makes these tests closer than the previous ones to the situations actually encountered in river hydraulics. Also in these cases, exact solutions can be computed using Bernoulli theorem and the conservation of momentum principle. A 50 m long and 10 m wide channel with rectangular cross section is considered. The bed profile is described by:

$$z_b(x) = 0.5 + 0.001x + \begin{cases} h_b \cos^2\left(\frac{\pi x}{10}\right) & -5 < x < 5 \\ 0 & \text{otherwise} \end{cases} \quad (33)$$

where h_b is the bump height. In the present tests the bed inclination without considering the bump is 0.1% and the Chézy roughness parameter is taken to be constant and equal to $20 \text{ m}^{1/2} \text{ s}^{-1}$. A constant discharge of $50 \text{ m}^3/\text{s}$ is imposed at the inflow boundary, while a constant water depth of 5 m is imposed at the outflow boundary. Two different bump heights are considered: $h_b = 2 \text{ m}$ and $h_b = 4 \text{ m}$. In the first case the flow is subcritical, while in the second case a transcritical flow with a steady shock is obtained. In figures 7 and 8 the results are compared to the exact solutions. The tolerance for the steady state is $\varepsilon = 10^{-7}$. In the case of subcritical flow $C_{vel} = 10$ is used, corresponding to a maximum celerity Courant number $C_{cel} = 48$; in the case of transcritical flow with a steady shock $C_{vel} = 1.9$ is used, corresponding to a maximum celerity Courant number $C_{cel} = 3.1$.

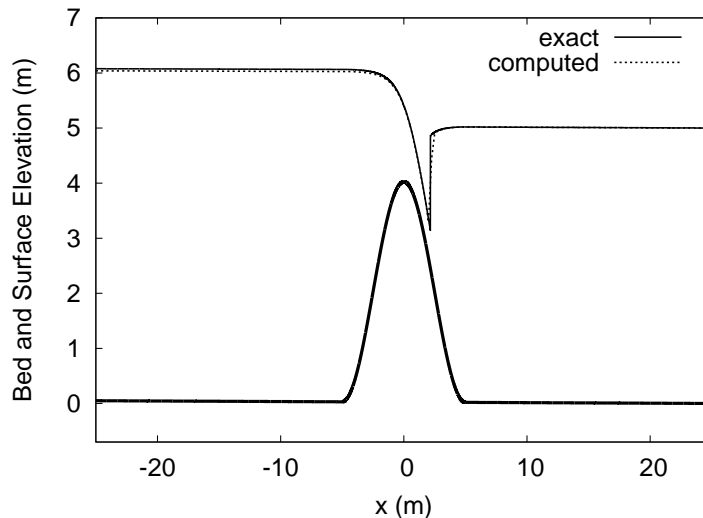


Figure 8: Transcritical flow over a bump with shock and friction: free surface elevation.

In both cases the agreement between exact and computed solution is very good. This tests demonstrate the capability of the method to describe frictional effects and to cope with large Courant numbers that allow a reduction of the computational costs.

6.4 Tidal wave in a short channel with variable depth and width

In this test the propagation of a tidal wave into a short channel with depth and width variations is considered. In [24] an asymptotic solution for $Fr \rightarrow 0$ is presented. Provided that the water depth h and the discharge per unit width q_l satisfy the boundary condition:

$$h(0, t) = \varphi(t) + \mathcal{H}(0) \quad (34)$$

$$q_l(L, t) = \psi(t) \quad (35)$$

where φ and ψ are given functions of time and \mathcal{H} is a reference level, the asymptotic solution for $Fr \rightarrow 0$ is:

$$h(x, t) = \varphi(t) + \mathcal{H}(x) \quad (36)$$

$$q_l(L, t) = \psi(t) + \frac{\varphi'(t)}{b(x)} \int_x^L b(s) ds \quad (37)$$

where $b(x)$ is the width of the rectangular channel and is a function of the x coordinate only. In this test we consider

$$\varphi(t) = 4 + 4 \sin \left[\pi \left(\frac{4t}{86400} - \frac{1}{2} \right) \right] \quad (38)$$

$$\psi(t) = 0. \quad (39)$$

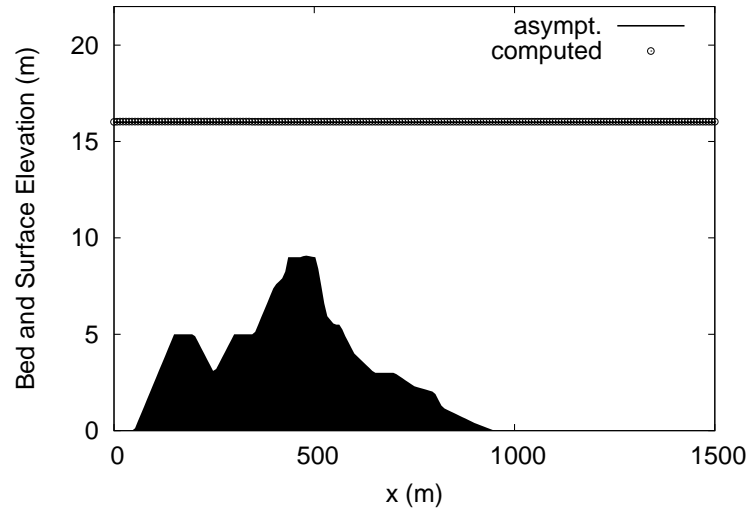


Figure 9: Tide in a short channel: free surface elevation and bathymetry.

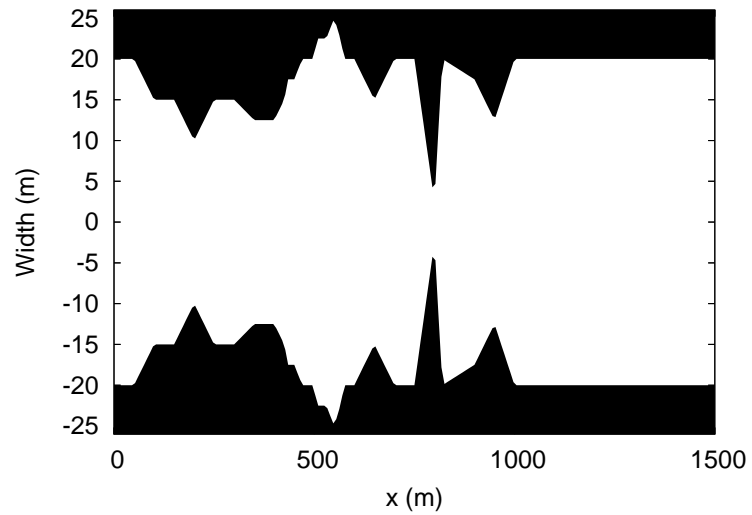


Figure 10: Channel width for tidal channel test case.

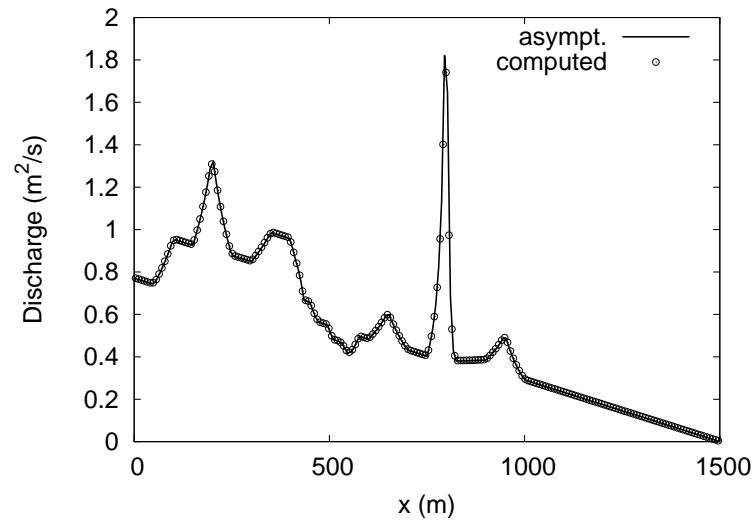


Figure 11: Tide in a short channel: discharge per unit width at time $t = 10\,800$ s.

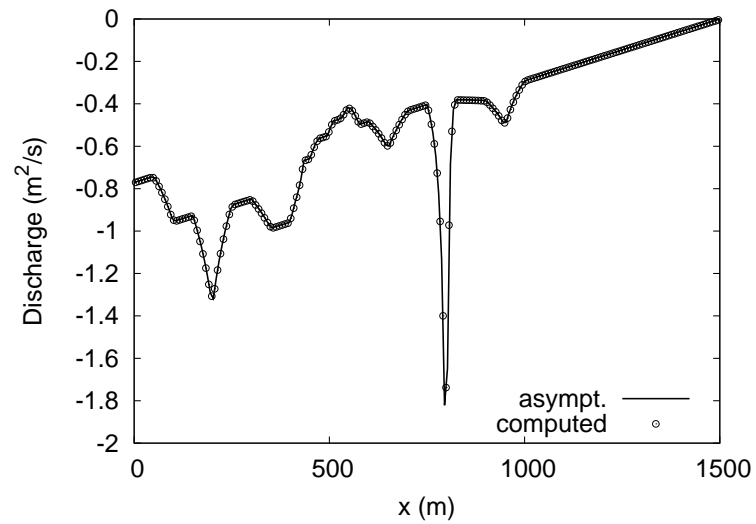


Figure 12: Tide in a short channel: discharge per unit width at time $t = 32\,400$ s.

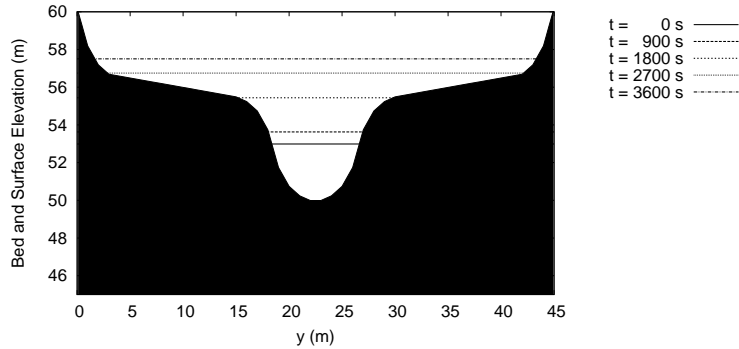


Figure 13: Flood wave in a channel with flood plains: computed free surface elevation at different time instants in the 11th section ($x = 100$ m).

This corresponds to a tidal wave of 8 m amplitude and to a null discharge at $x = L$. Moreover, the channel length is $L = 1\,500$ m, the Manning friction coefficient is $n = 0.1 \text{ s m}^{-1/3}$, the bottom profile and width functions are those proposed in [24] and represented in figures 9 and 10, respectively. The space discretization step is $\Delta x = 7.5$ m. These data correspond to the simulation presented in [19], [20] and [24]. Since the channel geometry is described by piecewise linear functions, the liquid area is interpolated at points $i + 1/2$ by means of a linear interpolation, thus using the upwind weighted interpolation with weight $p = 0.5$. The results are compared to the asymptotic solution at two time instants: $t_1 = 10\,800$ s which corresponds to the half-risen tide and the maximum positive velocities and $t_2 = 32\,400$ s which corresponds to the half-ebb tide and the maximum negative velocities. In figures 9 and 11, the free surface elevation and the discharge per unit width at time $t_1 = 10\,800$ s are presented. The free surface elevation at time $t_2 = 32\,400$ s is identical to that presented in figure 9; in figure 12 the discharge per unit width at time $t_2 = 32\,400$ s is presented. The agreement between exact and computed solution is always very good. During the simulation the maximum Courant number based on the velocity was 1.06 while the maximum Courant number based on the celerity was 98 corresponding to a time step $\Delta t = 62$ s; this time step is much larger than those used in [19], [20] and [24]. This test demonstrates the capability of the present method to give accurate results with time steps much larger than those used in traditional explicit schemes.

6.5 Flood wave in a channel with idealized flood plains

In this test, a channel is considered whose cross section is composed of a deeper main channel (thalweg) surrounded by two shallower flood plains. This represents an idealization of the flood plains actually encountered in many natural rivers. The bed inclination is 0.01%. The Chézy roughness parameter varies along the section being $30 \text{ m}^{1/2} \text{ s}^{-1}$ in the thalweg and $20 \text{ m}^{1/2} \text{ s}^{-1}$ in the flood plains. The domain is discretized into 1 001 uniformly spaced sections with $\Delta x = 10$ m. The initial conditions prescribe a discharge of $6.95 \text{ m}^3 \text{ s}^{-1}$ in the entire domain and a uniformly inclined sur-

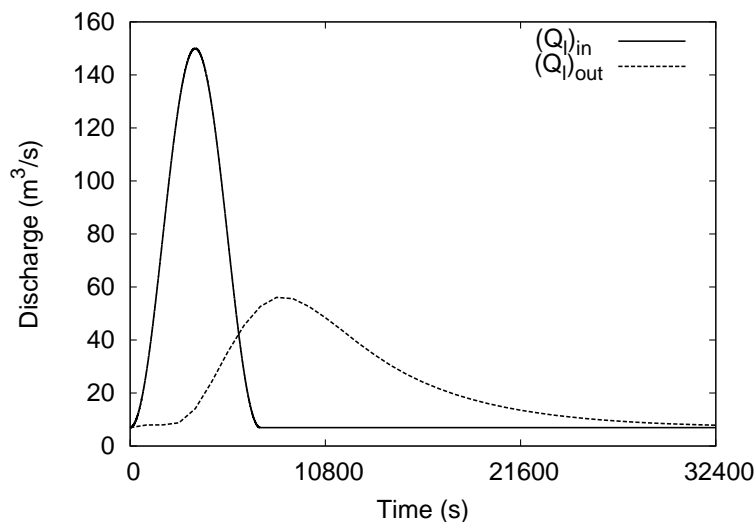


Figure 14: Flood wave in a channel with flood plains: discharge at the inflow and outflow sections.

face parallel to the river bed. A flood wave with maximum water discharge of $150 \text{ m}^3 \text{ s}^{-1}$ is imposed at the inflow boundary $x = 0$; the maximum discharge is reached in 1 hour and in the following hour the discharge returns to the uniform value $6.95 \text{ m}^3 \text{ s}^{-1}$ as shown in figure 14. At the outflow boundary $x = 10\,000$ a constant water depth $h = 3 \text{ m}$ is imposed.

The simulation is run to steady state ($\varepsilon = 10^{-7}$) using $C_{vel} = 1.5$. The steady state is reached in $54\,693 \text{ s}$ ($3\,758$ time steps). The maximum Courant number based on the celerity is 22, corresponding to a time step $\Delta t = 37 \text{ s}$. As the flood wave proceeds, the thalweg is filled and the flood plains are flooded. The flooding of the 11th section ($x = 100 \text{ m}$) is presented in figure 13. The Coriolis averaging coefficient β computed on the basis of the Lotter method is 1.04 when the water is entirely into the thalweg and reaches values up to 1.20 when the water is outside the thalweg, thus highlighting the importance of the section averaged formulation to capture some two dimensional effects. In order to evaluate the conservation properties of the method, the mass balance has been computed. At the end of the simulation the total mass loss is 31 m^3 , corresponding to 0.017% of the initial mass in the domain. This good result is achieved because the mass conservation equation is discretized by means of a conservative finite volume scheme and because the nonlinear dependence of the section liquid area on the free surface elevation has been taken into account (see section 5). The same simulation has been also performed without considering this nonlinear dependence of the system (thus considering a linearised expression of $V(\eta)$) and produced a total mass loss of $1\,197 \text{ m}^3$, corresponding to 0.664% of the initial mass in the domain. Finally, in figure 14 the discharges at the inflow and outflow boundaries are presented. The attenuation of the flood wave due to the flooding of the flood plains surrounding the thalweg is clearly displayed.



Figure 15: The Adda River basin.

7 Model validation: simulation of flooding events for the Adda River

In this section, we will present results on the simulation of flooding scenarios for the Adda River, which demonstrate the model effectiveness in a more realistic framework. The Adda River is located in the northern Italian region of Lombardy, see figure 15. It is the second largest contributor to the Po river and its basin amounts to approximately 11% of the Po river basin. The major water inflow is provided by the Como lake, but the contributions of the smaller Brembo and Serio tributaries can also be significant in general. Furthermore, the Martesana channel is derived from the Adda river approximately at the same point of the Brembo confluence. In our study, we have only considered the river tract downstream of the Como lake until Pizzighettone, see figure 16. This part of the river is about 115 km long and is comprised between Lavello and the Po river junction, located 16 km downstream of Pizzighettone. This choice was motivated by the availability of measurements at some of these locations.

The river has been described by means of 222 cross sections, shown in figure 17, where x denotes the distance from Lavello along the thalweg and the cross sections have been aligned with the centre of the coordinate system. The depth measurements along these sections were carried out by ADBPO (River Po Basin Authority) and are described in [1]. These cross sections are approximately 400 m apart from each other. Since the

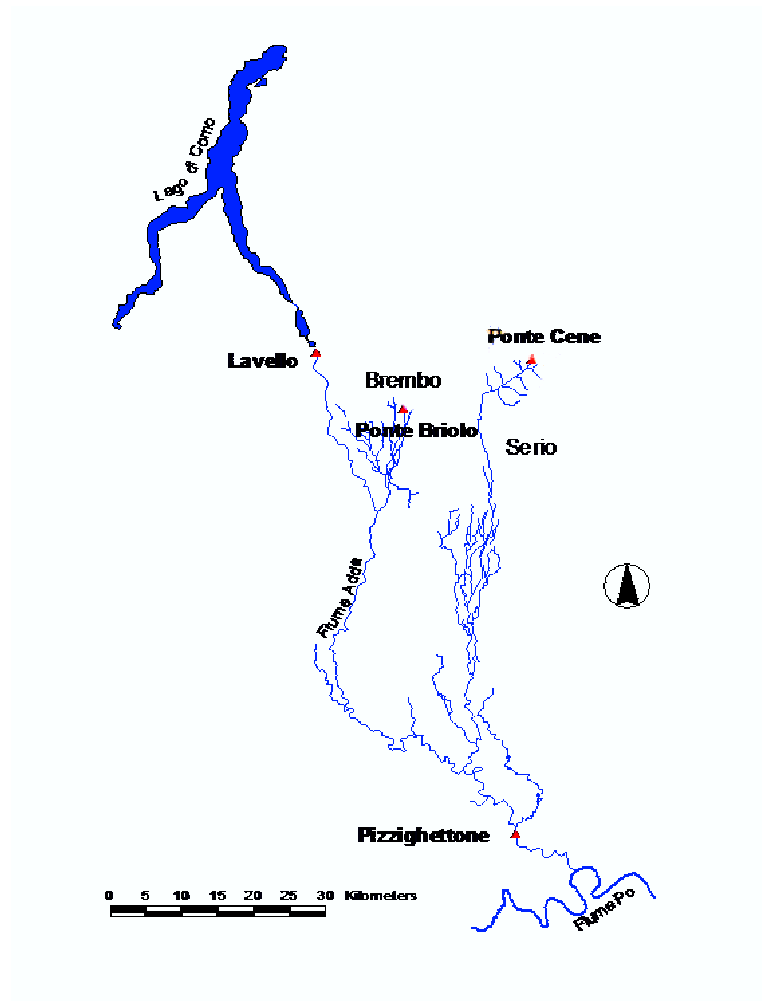


Figure 16: The hydrographic network including the Adda River. The most relevant measurement stations are highlighted.

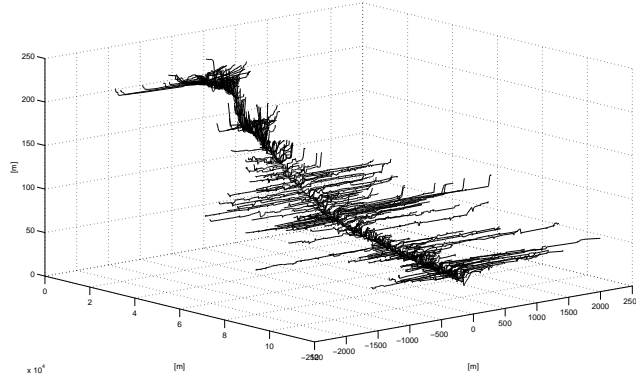


Figure 17: Cross sections describing the Adda River between the Como Lake and the junction with the Po River.

present implementation of the model cannot handle channel networks, we have only considered so far 171 sections describing the river between the Brembo–Martesana junction and Pizzighettone. The contribution of the Serio tributary has been neglected in this study. In this part of the river, the average yearly discharge is approximately $Q_l = 100 \text{ m}^3 \text{ s}^{-1}$ and the average slope is approximately 0.13%. Several bridges and other manufacts are present along the river, which have only been accounted for via their impact on the cross section geometry.

Semi-Lagrangian method		
Cross section [Km]	Absolute error [m]	Relative error [-]
196.96	0.002	0.0004
200.81	0.21	0.042
202.18	1.28	0.42
207.98	0.92	0.16
219.81	0.52	0.12
219.84	1.03	0.22
232.23	0.20	0.03
232.75	0.58	0.05
233.33	0.61	0.07
244.80	0.52	0.05
259.50	0.20	0.02
$\ \cdot\ _2$		0.096
$\ \cdot\ _\infty$		0.12

Table 1: Absolute and relative errors on maximum water levels for the semi-Lagrangian scheme, $C_{vel} = 3$

A key aspect in providing a realistic description of the river is the esti-

mation of the friction coefficients. These have been computed as described in section 3, starting from assigned local values of the Strickler coefficient along the cross sections. In particular, the Einstein–Horton method was used. These local Strickler coefficient values were expressed in terms of the Manning coefficient $n = 1/K$. For the estimate of the Manning coefficient, different approaches have been used for the deepest part of the cross sections, which are generally below the water surface in ordinary flow conditions, and for the flood plains, which are only flooded in case of exceptional events. For the deeper portions of the river cross sections, we have used the empirical Cowan formula $n = n_0 + n_1$ (see e.g. [9] for the description of this and other empirical formulae commonly used in these applications). Here, n_0 only depends on the typical sediment size in the river bed and n_1 on the presence of vegetation. We have neglected terms depending on section irregularities, cross section occlusions and river sinuosity, which are sometimes also included in the Cowan formula. In order to estimate n_0 , the Keulegan formula

$$n_0 = 0.0395d_{50}^{1/6} \quad (40)$$

was used (see e.g. [25]), where d_{50} is the median diameter of the sediment (expressed in meters). The data available to ADBPO showed that this parameter varies between 0.06 m close to Lavello to 0.005 m close to the confluence into the Po River. For the purpose of the present work, linear interpolation along the thalweg between these two values has been assumed to compute d_{50} values on each section. In the permanently wet areas, the parameter n_1 expressing dependence on vegetation was taken to be constant along each cross section and taking values comprised between $n_1 = 0.005 \text{ m}^{-1/3}\text{s}$ (modest vegetation cover) and $n_1 = 0.01 \text{ m}^{-1/3}\text{s}$ (large vegetation cover). For the flood plains, different values of the Manning coefficients have been considered, depending on the land use, which was identified on the basis of aerial survey data available in [1]. For urban and industrial areas, we used the value $n = 0.025 \text{ m}^{-1/3}\text{s}$, while we used the value $n = 0.035 \text{ m}^{-1/3}\text{s}$ for areas with agricultural use or with modest vegetation cover. For areas with dense vegetation, instead, the formula $n = \sqrt{n_{so}^2 + n_{veg}^2}$ was used, where n_{so} is the Manning coefficient for bare soil and

$$n_{veg} = n_{so} \sqrt{1 + \frac{\Lambda_\nu}{2g} \frac{1}{n_{so}} R_h^{1/3}} \quad (41)$$

where $\Lambda_\nu = A_p/a_x a_y$, A_p denotes the average plant cross section area, a_x is the average distance between plants in the direction of the main river flow, a_y the average distance between plants in the direction perpendicular to the main flow.

Following the same approach of [2], two sets of simulations have been performed: firstly, a calibration run was carried out, in order to identify values of the friction coefficients that allowed to reproduce as accurately as possible water level measurements concerning a recent flood. Using these values for the friction coefficients, a validation run was then carried out,

which shows how the model correctly reproduces hydrological estimates of flooding events with specified return times.

The discharge and water level data available for the November 2002 flood were used for a first model calibration. The data we used were recovered from the measurements available for the time period between November 20th and December 2nd 2002 reported in [2]. In the simulation we performed, the initial datum was given by a steady state profile computed on the basis of the energy balance equation (see e.g. [9]) assuming a discharge of $Q_t = 727 \text{ m}^3 \text{ s}^{-1}$ and a water depth at the outflow of 7.2m. These values correspond to the initial value of the discharge and water level time series at the upstream and downstream boundaries, respectively, see figure 18. The Manning coefficient values in the deeper parts of the river sections were used as calibration parameters, within the bounds reviewed above. As in previous studies carried out by ADBPO (see [2]), the calibration was aimed at minimizing the difference between computed and measured values for the maximum water levels achieved at 11 specific river locations. Some of these do not correspond to the cross sections used in the numerical simulation, so that the computed water levels were then linearly interpolated at the appropriate location. The simulation was carried out with different time steps, yielding a range of velocity Courant numbers comprised between $C_{vel} = 0.8$ and $C_{vel} = 3$. The water level errors obtained with the semi-Lagrangian and upwind advection schemes are reported in tables 1 and 2, respectively. It can be observed that both schemes yield accurate results on most of the sections for which measured flood data are available, demonstrating the effectiveness of the semi-implicit, semi-Lagrangian approach in reducing the computational cost while maintaining the same level of accuracy as explicit schemes. Indeed, these results are entirely analogous to those of the simulations reported in [2], which were obtained with a fully explicit, flux-form discretization. Larger errors, however, are still present in some of the measured sections. These are related to the fact that the presence of artificial manufacts such as bridges was not fully accounted for in our simulation.

In a second set of model runs, the Manning coefficient values resulting from the calibration on the November 2002 flood were used to simulate flooding scenarios, based on synthetic hydrograms (discharge time series) computed by hydrological estimation for the river Adda. These datasets represent flood events with assigned return times, reconstructed on the basis of the available time series of rainfall and discharge data keeping into account the geomorphology of the river basin. The synthetic hydrograms for the Adda river we used are reported in [2] and were derived using the methodology proposed in [15]. An example of the discharge profiles at the upstream boundary is shown in figure 20. In the simulation we performed, these data were used as upstream boundary conditions, while the computed results are compared with analogous hydrological estimates at sections further downstream. The downstream boundary was placed in this simulation approximately 10 km downstream of the Pizzighettone section used in the calibration run. The hydrograms computed at two different locations by the semi-Lagrangian method with Courant number 2 for return times of 20 and 200 years are compared with the hydrological estimates in figures 21

Upwind		
Cross section [Km]	Absolute error [m]	Relative error [-]
196.96	0.002	0.0004
200.81	0.22	0.042
202.18	1.27	0.42
207.98	0.92	0.16
219.81	0.34	0.08
219.84	0.85	0.18
232.23	0.37	0.06
232.75	0.46	0.04
233.33	0.48	0.05
244.80	0.62	0.06
259.50	0.29	0.04
$\ \cdot \ _2$		0.091
$\ \cdot \ _\infty$		0.12

Table 2: Absolute and relative errors on maximum water levels for the upwind scheme, $C_{vel} = 0.8$

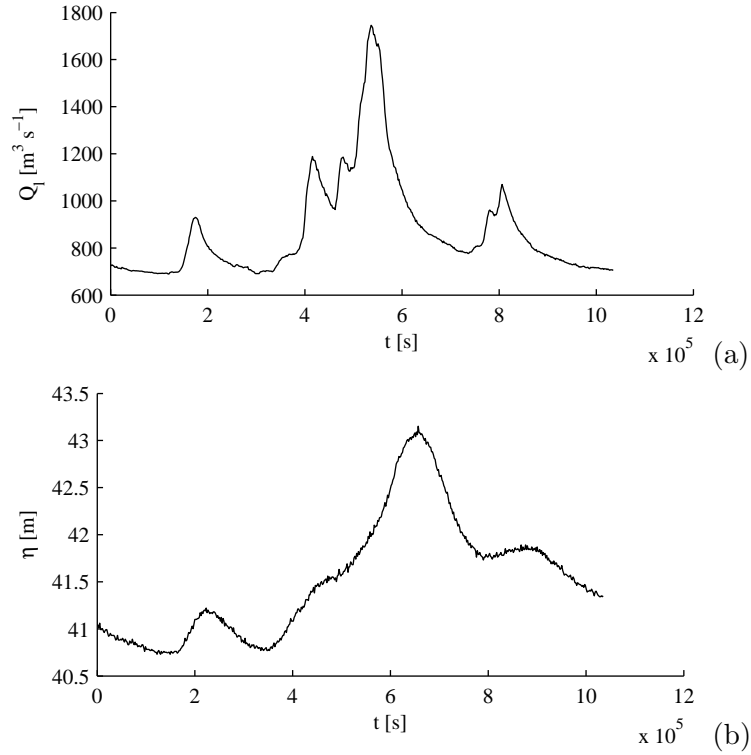


Figure 18: (a) Discharge time series for the upstream boundary condition; (b) water level time series for the downstream boundary condition.

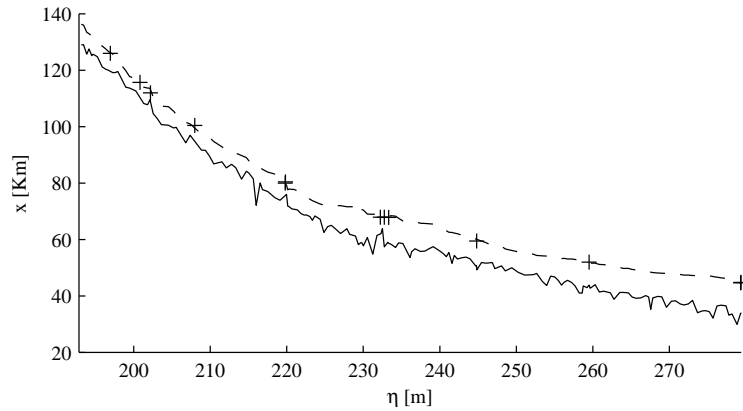


Figure 19: Comparison of computed (dotted line) and measured (crosses) maximum water levels. The continuous line represents the thalweg bottom height.

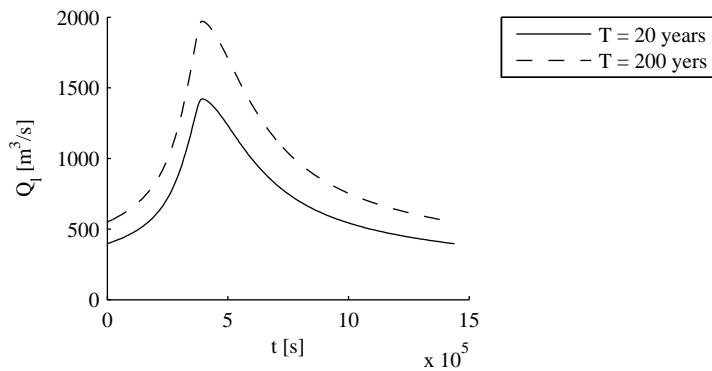


Figure 20: Synthetic hydrograms at the upstream boundary of the computational domain for floods with return times $T = 20$ years and $T = 200$ years.

and 22, respectively. It can be observed that the peak values are correctly reproduced in amplitude. Away from the peak, the computed values are slightly larger than the hydrological estimates. This effect is due indeed to a slight underestimation of the discharges in the hydrological estimates, which was also observed in the analogous simulations presented in [2] and computed with an explicit, flux-form method.

8 Conclusions

An efficient and robust numerical method for the solution of the section averaged equations of open channel flow has been presented and discussed. The use of a semi-implicit, semi-Lagrangian time discretization technique based on the approaches proposed in [6], [7], [8], [18] for the two and three

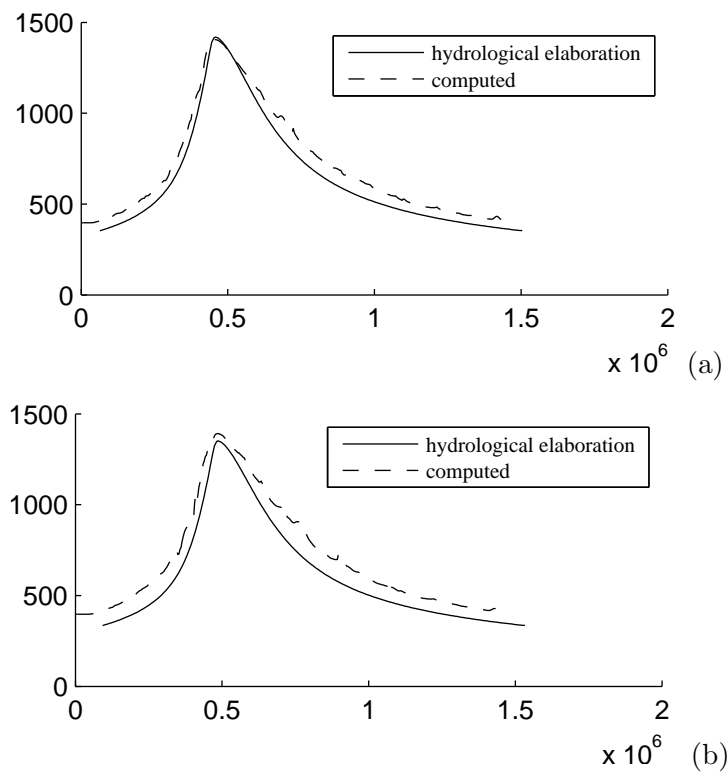


Figure 21: Comparison between numerically computed and statistically simulated hydrograms for a return time of 20 years at (a) Serio confluence (b) Pizzighettone.

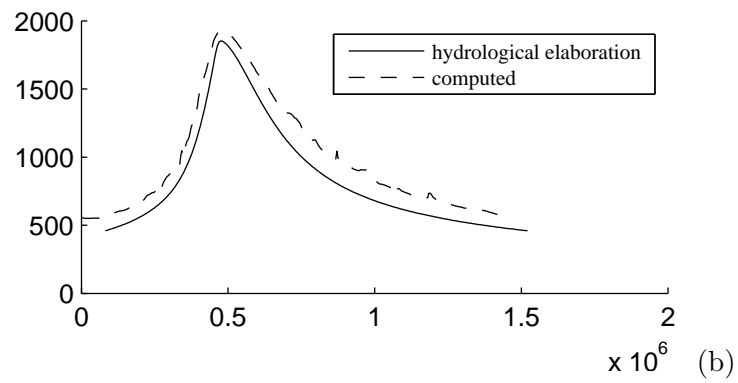
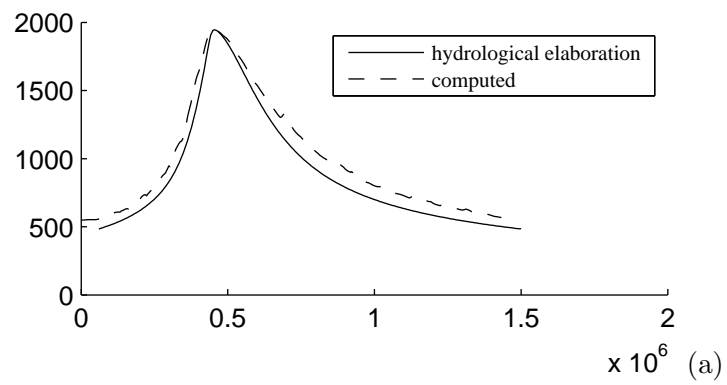


Figure 22: Comparison between numerically computed and statistically simulated hydrograms for a return time of 20 years at (a) Serio confluence (b) Pizzighettone.

dimensional shallow water equations yields an unconditionally stable numerical method, whose time step can be chosen based on accuracy considerations, rather than stability restrictions. The stable and accurate time discretization technique allows to reduce substantially the computational costs, by employing time steps much larger than those used with standard explicit discretizations. In the same context, also an upwind discretization for the momentum equation has been introduced. Furthermore, the method is based on the section-averaged equations of river flow, thus allowing to handle arbitrarily shaped sections and to recover some two dimensional information across the available sections.

A wide range of benchmarks relevant for river hydraulics applications has been computed, along with a more realistic application to simulation of flooding scenarios for the river Adda. The results obtained in these tests show that the method is capable of achieving results entirely analogous to those of more conventional explicit, flux-form discretizations, while achieving a remarkably superior computational efficiency. The robustness and efficiency characteristics of the method make it especially appealing for computationally intensive simulations. In particular, an extension of the present method to the mobile bed case is presently being developed, to be used for sediment transport simulations and river morphology studies. Finally, it is planned to extend the present model to a hybrid 1D-2D model along the lines of [16], [17], exploiting the model capability of handling arbitrarily shaped sections.

Acknowledgements

We would like to acknowledge many useful conversations with A. Armanini, V. Casulli, A. Decoene, L. Fraccarollo, E. Miglio, A. Quarteroni, M.C. Rulli and P. Zanolli on the topics studied in this paper. A. Deponti also acknowledges the warm hospitality at MOX. The first version of the section averaged model was developed at University of Trento and CUDAM by G. Rosatti. The hydrologic and hydraulic data on the river Adda were supplied by ADBPO (River Basin Authority for the Po River); in particular, we would like to thank dr. T. Simonelli for his help and assistance with the Adda datasets.

References

- [1] ADBPO. Studio della sistemazione idraulica del fiume Adda nel tratto da Olginate alla confluenza nel Po. Technical report, Po River Basin Authority, Parma, 2002-3.
- [2] ADBPO. Rapporto sulla piena del Novembre 2002 in Lombardia. Technical report, Po River Basin Authority, Parma, 2003.
- [3] E. Aldrighetti and P. Zanolli. A high resolution scheme for flow in open channels with arbitrary cross-section. *International Journal of Numerical Methods in Fluids*, 47:817–824, 2005.

- [4] L. Bonaventura. A semi-implicit, semi-lagrangian scheme using the height coordinate for a nonhydrostatic and fully elastic model of atmospheric flows. *Journal of Computational Physics*, 158:186–213, 2000.
- [5] H. Capart, T.I. Eldho, S.Y. Huang, D.L. Young, and Y. Zech. Treatment of natural geometry in finite volume river flow computations. *J. Hydraulic Engineering*, 129(5):385–393, 2003.
- [6] V. Casulli. Semi-implicit finite difference methods for the two dimensional shallow water equations. *Journal of Computational Physics*, 86:56–74, 1990.
- [7] V. Casulli and E. Cattani. Stability, accuracy and efficiency of a semi-implicit method for three-dimensional shallow water flow. *Computers and Mathematics with Applications*, 27(4):99–112, 1994.
- [8] V. Casulli and P. Zanolli. A conservative semi-implicit scheme for open channel flows. *Journal of Applied Science and Computations*, 5:1–10, 1998.
- [9] V.T. Chow. *Open Channel Hydraulics*. McGraw Hill, 1959.
- [10] A. Deponti, L. Bonaventura, L. Fraccarollo, E. Miglio, and G. Rosatti. Analysis of hyperbolic systems for mobile-bed, free-surface flow modelling in arbitrary cross sections. Technical Report 06/2007, MOX - Dipartimento di Matematica, Politecnico di Milano, 2007.
- [11] T. Gallouët, J.M. Hérard, and N. Seguin. Some approximate godunov schemes to compute shallow-water equations with topography. *Computers & Fluids*, 32:479–513, 2003.
- [12] N. Goutal and F. Maurel. Proceedings of the 2nd Workshop on Dam-Break Wave Simulations. Technical Report HE-43/97/016/A, Electricité de France, Département Laboratoire National d’Hydraulique, Groupe Hydraulique Fluviale, 1997.
- [13] B. Gustafsson, H.O. Kreiss, and J. Olinger. *Time dependent problems and difference methods*. Wiley, 1995.
- [14] R. J. Leveque. *Finite Volume Methods for Hyperbolic Problems*. Cambridge University Press, Cambridge, UK, 2002.
- [15] U. Maione, P. Mignosa, and M. Tomirotti. Regional estimation of synthetic design hydrographs. *International Journal of River Basin Management*, 1(2):151–163, 2003.
- [16] E. Miglio, S. Perotto, and F. Saleri. Model coupling techniques for free-surface flow problems: Part I. *Nonlinear Analysis*, 63:1885–1896, 2005.
- [17] E. Miglio, S. Perotto, and F. Saleri. Model coupling techniques for free-surface flow problems: Part II. *Nonlinear Analysis*, 63:1897–1908, 2005.
- [18] E. Miglio, A. Quarteroni, and F. Saleri. Finite element approximation of quasi-3d shallow water equations. *Comp. Methods in Applied Mechanics and Engineering*, 174:355–369, 1999.
- [19] T.C. Rebollo, A.D. Delgado, and E.D.F. Nieto. A family of stable numerical solvers for the shallow water equations with source terms.

Computer methods in applied mechanics and engineering, 192:203–225, 2003.

- [20] T.C. Rebollo, E.D.F. Nieto, and M.G. Mármol. A flux-splitting solver for shallow water equations with source terms. *International Journal of Numerical Methods in Fluids*, 42:23–55, 2003.
- [21] G. Rosatti and L. Fraccarollo. A well-balanced approach for flows over mobile-bed with high sediment-transport. *Journal of Computational Physics*, 220(1):312–338, 2006.
- [22] E. Toro. *Shock-Capturing Methods for Free-Surface Shallow Flows*. Wiley, 2001.
- [23] E.F. Toro. *Riemann solvers and numerical methods for fluid dynamics*. Springer-Verlag, 1997.
- [24] M.E. Vázquez-Cendón. Improved treatment of source terms in upwind schemes for the shallow water equations in channels with irregular geometry. *Journal of Computational Physics*, 148:497–526, 1999.
- [25] B.C. Yen. *Channel Flow Resistance: Centennial of Manning’s Formula*. Water Resources Publications, Littleton, CO, 1992.
- [26] J.G. Zhou, D.M. Causon, C.G. Mingham, and D.M. Ingram. The surface gradient method for the treatment of source terms in the shallow-water equations. *Journal of Computational Physics*, 168:1–25, 2001.